

Biomagnetic flow in a curved square duct under the influence of an applied magnetic field

P.K. Papadopoulos¹ and E.E. Tzirtzilakis^{*2}

¹Department of Engineering Sciences, University of Patras, GR 26500 Patras, Greece

²Department of Mathematics, Division of Applied Analysis, University of Patras, GR 26500 Patras, Greece
e-mail address: p.papado@des.upatras.gr & tzirtzi@iconography.gr

Abstract

The laminar incompressible fully developed biomagnetic (blood) flow in a curved square duct under the influence of an applied magnetic field is studied. The mathematical formulation is based on the model of BFD which is consistent with the principles of ferrohydrodynamics. According to this formulation blood is considered as an electrically non-conducting, homogeneous and Newtonian magnetic fluid. For the numerical solution of the problem, which is described by a coupled, non-linear system of PDEs, with their appropriate boundary conditions, the SIMPLE method is used. The results indicate that the axial velocity, as well as the secondary flow at the transverse plane are appreciably influenced and indicate that the magnetic field could be used for controlling the blood flow by magnetic means.

* Correspondence address: 18 Ersis, Galatsi, 11146 Athens, Greece.

INTRODUCTION

Biomagnetic Fluid Dynamics (BFD) is a relatively new area in fluid mechanics investigating the fluid dynamics of biological fluids in the presence of magnetic field. The application of a magnetic field on the flow of biological fluids is investigated for bioengineering and medical applications concerning drug targeting, cell separation or reduction of blood flow during surgeries [1]~[5].

A biomagnetic fluid is a fluid that exists in a living creature and its flow is influenced by the presence of a magnetic field. The most characteristic biomagnetic fluid is blood, which behaves as a magnetic fluid, as suggested by [7], due to the complex interaction of the intercellular protein, cell membrane and the haemoglobin, a form of iron oxides, which is present at a uniquely high concentration in the mature red blood cells, while its magnetic property is affected by factors such as the state of oxygenation. As a consequence the red blood cells behave like magnetic dipoles in the plasma. The orientation of erythrocytes with their disk plane parallel to the magnetic field has been verified in [6]~[11]. Blood possesses the property of diamagnetic material when oxygenated and paramagnetic when deoxygenated [12], with magnetic susceptibility 3.5×10^{-6} and -6.6×10^{-7} for the venous and arterial blood, respectively [13], [14]. With the addition of artificially synthesized magnetic micro spheres, blood behaves like ferromagnetic material [5]. Further experiments have been made using relatively weak magnetic field (1.8 Tesla) and low temperatures (75-295 °K) [15]. Strong magnetic fields (8 Tesla) were also used on a living rat whose blood flow and temperature reduced [16] and experiments have shown that for a magnetic field of the same strength, the flow rate in a tube was reduced by 30% [17].

The mathematical model of BFD has been developed on the principles of Ferrohydrodynamics (FHD). According to this formulation, blood is actually considered as an electrically non conducting magnetic fluid and the flow is affected by the magnetization of the fluid in the magnetic field. Thus, the arising force which is due to magnetization depends on the existence of a spatially varying magnetic field. This formulation

opposes to the well known formulation in MagnetoHydroDynamics (MHD), which deals with conducting fluids and the corresponding mathematical model ignores the effect of polarization and magnetization [1], [5], [13], [17]~[25].

Thus, according to the above mentioned mathematical model, biofluids are considered as electrically poor conductors and the flow is affected only by the magnetization of the fluid in a spatially varying magnetic field. It is noted that in all the above formulations the biofluid is considered homogeneous with Newtonian behaviour. Consequently, the present BFD model refers to Newtonian blood flow like the one in large arteries.

The hydrodynamic problem of flow in a curved duct has been investigated numerically in [32]~[39] using the stream function vorticity formulation, SIMPLE and the recently developed CVP method. Experimental data about developing and fully developed flows in curved square ducts have also been given in [40] and [41]. The fully developed biomagnetic fluid flow in a straight rectangular duct has been investigated in [42] and results for magnetic fluid flow in the same geometry are also given in [19].

In the present study the laminar, incompressible, fully developed viscous flow of a biomagnetic fluid (blood) in a curved rectangular duct is numerically studied with the use of the SIMPLE method. The blood is considered as a homogeneous and Newtonian fluid as in [43], [44] and the magnetization M is considered as a function of the magnetic field intensity H .

The results concerning the flow rate, the axial velocity and the secondary flow in the transverse plane, show that the flow is appreciably influenced by the magnetic field. The presence of the magnetic field affects the secondary flow whereas the axial velocity is reduced near the area of the magnetic source. The effect also of the magnetic field is dependent on the position of the magnetic source and can result in asymmetric flow. These results indicate that the magnetic field could be used for controlling the blood flow by magnetic means and encourage further studying for possible medical and bioengineering applications.

MATHEMATICAL FORMULATION

The problem under consideration is the Newtonian, steady, laminar, fully developed flow inside a curved square duct under the influence of an applied magnetic field. The length and height of the duct is a and the radius of curvature is R . The magnetic field is generated by an electric current going through a thin wire placed parallel to the longitudinal axis at the position (x_s, y_s) outside of the duct depicted in Figure 1 by the dash-dot line. For the study of the flow a toroidal coordinate system was used. The flow configuration is pictured in Figure 1. The contours of the spatially varying magnetic field of strength H are shown in the ABCD plane of the cross section where the flow is studied.

According to the mathematical model of BFD [1], [5], [13], [17], [18] which is consistent with the principles of FHD [19]~[25], blood is assumed as a homogeneous Newtonian fluid. The Lorentz force due to the electrical conductivity of blood is considered negligible compared to the magnetization force and this assumption is further investigated in a latter section. Thus, blood is also considered electrically non-conducting fluid. Moreover, equilibrium magnetization is assumed which is an assumption that proved to be valid after experiments in [13] and the apparent viscosity due to the application of the magnetic field is considered negligible.

The Cartesian system (X, Y, Z) is related to the toroidal one $(\bar{x}, \bar{y}, \bar{z})$ by the relations

$$X = (R + \bar{x})\cos(\bar{z}/R) \quad Z = (R + \bar{x})\sin(\bar{z}/R) \quad Y = \bar{y} \quad (1)$$

Hence at the fully developed flow, the dimensional velocity components of $\vec{V} = (\bar{u}, \bar{v}, \bar{w})$ and the pressure \bar{P} are governed by the mass conservation and the fluid momentum equations at the $\bar{x}, \bar{y}, \bar{z}$ directions, which are given respectively by:

Continuity equation

$$\frac{\partial \bar{u}}{\partial \bar{x}} + \frac{\partial \bar{v}}{\partial \bar{y}} + \bar{\kappa} C \bar{u} = 0 \quad (2)$$

Momentum equation in the x axis

$$\rho \left(\frac{\partial \bar{u}^2}{\partial \bar{x}} + \frac{\partial (\bar{u}\bar{v})}{\partial \bar{y}} - \bar{\kappa} C (\bar{w}^2 - \bar{u}^2) \right) = -\frac{\partial \bar{p}}{\partial \bar{x}} + \mu \left(\frac{\partial^2 \bar{u}}{\partial \bar{x}^2} + \frac{\partial^2 \bar{u}}{\partial \bar{y}^2} + \bar{\kappa} C \frac{\partial \bar{u}}{\partial \bar{x}} - (\bar{\kappa} C)^2 \bar{u} \right) + \mu_0 \bar{M} \frac{\partial \bar{H}}{\partial \bar{x}} \quad (3)$$

Momentum equation in the y axis

$$\rho \left(\frac{\partial (\bar{u}\bar{v})}{\partial \bar{x}} + \frac{\partial \bar{v}^2}{\partial \bar{y}} + \bar{\kappa} C \bar{u}\bar{v} \right) = -\frac{\partial \bar{p}}{\partial \bar{y}} + \mu \left(\frac{\partial^2 \bar{v}}{\partial \bar{x}^2} + \frac{\partial^2 \bar{v}}{\partial \bar{y}^2} + \bar{\kappa} C \frac{\partial \bar{v}}{\partial \bar{x}} \right) + \mu_0 \bar{M} \frac{\partial \bar{H}}{\partial \bar{y}} \quad (4)$$

Axial momentum equation in the z axis

$$\rho \left(\frac{\partial (\bar{u}\bar{w})}{\partial \bar{x}} + \frac{\partial (\bar{v}\bar{w})}{\partial \bar{y}} + 2\bar{\kappa} C \bar{u}\bar{w} \right) = -\bar{J} \frac{d\bar{p}_a}{dz} + \mu \left(\frac{\partial^2 \bar{w}}{\partial \bar{x}^2} + \frac{\partial^2 \bar{w}}{\partial \bar{y}^2} + \bar{\kappa} C \frac{\partial \bar{w}}{\partial \bar{x}} - (\bar{\kappa} C)^2 \bar{w} \right) \quad (5)$$

where $\bar{\kappa}$ is the curvature defined as $\bar{\kappa} = 1/(R + a/2)$ the term C is defined as $C = 1/(1 + \bar{\kappa}\bar{x})$.

Magnetic Field Equations

$$\nabla \times \bar{H} = \bar{J} = 0 \quad (6)$$

$$\nabla \cdot \bar{B} = \nabla \cdot (\bar{H} + \bar{M}) = 0$$

In the above dimensional equations, B is the magnetic field induction, H is the magnetic field strength intensity, ρ is the fluid density, J is the induced current, μ is the viscosity and μ_0 is the magnetic permeability of vacuum.

For the magnetization equation the following linear equation for isothermal cases [17], [21], [24] is used.

$$\bar{M} = \chi \bar{H} \quad (7)$$

where χ is a constant called magnetic susceptibility.

The boundary conditions are

$$\bar{y} = 0 \quad \text{or} \quad \bar{y} = a \quad \text{and} \quad 0 \leq \bar{x} \leq a \quad : \quad \bar{u} = \bar{v} = \bar{w} = 0 \quad (8)$$

$$\bar{x} = 0 \quad \text{or} \quad \bar{x} = a \quad \text{and} \quad 0 \leq \bar{y} \leq a \quad : \quad \bar{u} = \bar{v} = \bar{w} = 0 \quad (9)$$

where a is the length and the height of the square cross-section.

The magnitude $[H]$, of the magnetic field intensity, is given by

$$[H](\bar{x}, \bar{y}) = \frac{\gamma}{2\pi} \frac{1}{(\bar{x} - \bar{x}_s)^2 + (\bar{y} - \bar{y}_s)^2} \quad (10)$$

where γ is the magnetic field strength at the source, namely the point $(\bar{x} = \bar{x}_s, \bar{y} = \bar{y}_s)$.

By introducing the non-dimensional variables

$$x = \frac{\bar{x}}{a} \quad y = \frac{\bar{y}}{a} \quad z = \frac{\bar{z}}{a} \quad u = \frac{\bar{u}a}{\nu} \quad v = \frac{\bar{v}a}{\nu} \quad w = \frac{\bar{w}a}{\nu} \quad (11)$$

$$H = \frac{\bar{H}}{H_0} \quad p = \frac{\bar{p}}{\rho \nu^2 / a^2} \quad \kappa = \bar{\kappa} a$$

where ν is the kinematic viscosity, ρ is the density, $H_0 = [H](\bar{x}_0, \bar{y}_0)$, the governing equations (2)~(5) are transformed to the following equations:

Continuity equation

$$\frac{\partial u}{\partial x} + \frac{\partial v}{\partial y} + \kappa C u = 0 \quad (12)$$

Momentum equation in the x axis

$$\frac{\partial u^2}{\partial x} + \frac{\partial(uv)}{\partial y} = -\frac{\partial p}{\partial x} + \frac{\partial^2 u}{\partial x^2} + \frac{\partial^2 u}{\partial y^2} + \kappa C \frac{\partial u}{\partial x} - (\kappa C)^2 u + \kappa C(w^2 - u^2) + Mn H \frac{\partial H}{\partial x} \quad (13)$$

Momentum equation in the y axis

$$\frac{\partial(uv)}{\partial x} + \frac{\partial v^2}{\partial y} = -\frac{\partial p}{\partial y} + \frac{\partial^2 v}{\partial x^2} + \frac{\partial^2 v}{\partial y^2} + \kappa C \frac{\partial v}{\partial x} - \kappa C u v + Mn H \frac{\partial H}{\partial y} \quad (14)$$

Axial momentum equation in the z axis

$$\frac{\partial(uw)}{\partial x} + \frac{\partial(vw)}{\partial y} = -C \frac{dp_a}{dz} + \frac{\partial^2 w}{\partial x^2} + \frac{\partial^2 w}{\partial y^2} + \kappa C \frac{\partial w}{\partial x} - (\kappa C)^2 w - 2\kappa C u w \quad (15)$$

The boundary conditions are

$$y = 0 \quad \text{or} \quad y = 1 \quad \text{and} \quad 0 \leq x \leq 1 \quad : \quad u = v = w = 0 \quad (16)$$

$$x = 0 \quad \text{or} \quad x = 1 \quad \text{and} \quad 0 \leq y \leq 1 \quad : \quad u = v = w = 0 \quad (17)$$

where $Mn = \frac{a^2 \bar{\mu}_o \chi \bar{H}_o^2}{\bar{v}^2 \bar{\rho}}$ is the magnetic number.

For a specific fluid ($v, \rho, \chi, \mu_o = \text{const.}$) and a specific flow problem ($a = \text{const.}$), variation of the Mn number means variation of the magnetic field intensity H_o . Thus increasing the Mn number means increment of the magnetic field intensity at the magnetic source.

In internal flows with small transversal velocities the variation of the pressure in the transversal plain is small and its gradient in the axial direction can be ignored in the corresponding momentum equation. Thus the pressure p_0 may be split in two parts, the axial p_a and the transversal pressure distribution p ($p_0(x,y,z) = p(x,y) + p_a(z)$) and with the assumption of the fully developed flow it is concluded that the axial pressure gradient dp_a/dz (which will be symbolized by Pz) can be regarded as uniform over the cross-section and constant in the longitudinal direction. The mean axial velocity, which in the current nondimensional form coincides with the Reynolds number, is given by:

$$w_m = \frac{\int_A w dA}{\int_A dA} \quad (18)$$

where A is the area of the cross-section and $Re = w_m$.

NUMERICAL SIMULATION

The governing equations were solved according to the SIMPLE method in the finite volume formalism by use of a staggered grid [45]. The convection and diffusion terms were discretized with the second order central differences scheme. For the solution of the uncoupled equations (13), (14) and (15) the successive

line under-relaxation (SLUR) solver was adopted together with the well-known tridiagonal matrix algorithm (TDMA). Convergence of the iteration procedure was achieved when the following criterion was satisfied for all nodes:

$$\frac{\|\phi_{ij}^{k+1} - \phi_{i\xi}^k\|_{\infty}}{\|\phi_{ij}^{k+1}\|_{\infty}} \leq 10^{-5}$$

where ϕ stands for velocities u, v, w , the subscripts i, j represent the x and y coordinates and the superscript k is the k th iteration. It was necessary to use an under-relaxation factor according to [45], ranging between 0.3 and 0.1 for the various computational cases in order to make the solution converge.

It has been found that under the influence of 8T magnetic field, blood ($\bar{\rho}=1050\text{kg}/\text{m}^3$, $\bar{v}=3.1\times 10^{-6}\text{m}^2\text{sec}^{-1}$ [47]) has reached magnetization of 40Am^{-1} [13].

From the definition of the Mn it is apparent that

$$\text{Mn} = \frac{a^2 \mu_0 \chi \bar{H}_o^2}{\bar{v}^2 \bar{\rho}} = \frac{a^2 \bar{B}_o \bar{M}_o}{\bar{v}^2 \bar{\rho}} \quad (19)$$

where $\bar{\mu}_0$ is the magnetic permeability of vacuum equal to $4\pi\times 10^{-7}$, B_o is the magnetic field induction to $H_o(x_o, y_o)$ and M_o the corresponding magnetization. Thus, for $B_o=8\text{T}$ and $a=1.2\times 10^{-2}\text{m}$, which corresponds to cross-section of a large vessel, it is apparent that $\text{Mn} \approx 5\times 10^6$.

It is also noted that in many applications, especially in magnetic drug targeting, magnetic nanoparticles are injected in blood in order to use them as a drug delivery system for localized therapy [3], [4]. Similar nano-spheres have been constructed in order to increase the magnetization of blood [5]. These nano-spheres attached to the erythrocytes and as a consequence the magnetization of blood could be increased by one or two orders of magnitude. Thus, with the addition of magnetic nanoparticles in blood it is possible to achieve the same magnetic number using magnetic field of the order of 1T.

Blood particularly, exhibits considerably high static electrical conductivity, which is hematocrit and temperature dependent. Over the above, the electrical conductivity of blood varies as the flow rate varies [26]~[28]. The electrical conductivity $\bar{\sigma}$ of stationary blood was measured to be 0.7sm^{-1} . The electrical

conductivity of flowing blood is always greater than that of the stationary and the increment for medium shear rates is about 10% and it further increases with the increment of the hematocrit [26]. So, it can be assumed for simplicity that the electrical conductivity of blood is temperature independent and equal to 0.8 sm^{-1} .

The Lorentz force per unit volume due to the electrical conductivity of blood, arises in the direction of the flow and perpendicularly to the direction of the application of the magnetic field. This force is well known in MHD [29]~[31] and is expressed by the term $-\sigma \bar{B}^2 \bar{w}$. So, in order to include the Lorentz force in the problem under consideration we could add this term on the right hand side of equation (5). After the introduction of the non-dimensional variables (11), the term $-Mn_M H^2 w$ arises at the right hand side of equation (15). The Mn_M is a new magnetic number which arises due to the adopted Lorentz force of MHD and

$$Mn_M = \frac{a^2 \sigma \bar{\mu}_o^2 \bar{H}_o^2}{\bar{\nu} \bar{\rho}} = \frac{a^2 \sigma \bar{B}_o^2}{\bar{\nu} \bar{\rho}}.$$

After calculations in the flow domain of the term $-Mn_M H^2 w$ due to MHD and the term $Mn H(\partial H/\partial x)$ of FHD it is obtained that the term due to MHD is at least two orders of magnitude less than the corresponding one of FHD for the specific magnetic field intensity H used. Moreover, after further calculations with the new term of MHD added in the governing equations no differences were found in the flow domain. Thus, the assumption of blood as an electrically non-conducting fluid is valid for the problem under consideration.

As far as the hydrodynamic flow ($Mn=0$) in a curved duct (various values of κ) is concerned, computations were performed using various grid sizes and Re numbers in order to establish grid independence. The numerical tests involved mesh sizes of 30×30 , 46×46 and 60×60 grid cells and the results showed a maximum discrepancy of 0.85% between the first two grids and 0.5% between the two latter. Thus, a 46×46 grid was chosen for the computations as it combines accuracy with considerable computational economy.

As far as the effect of the magnetic field is concerned, calculations for a straight duct ($\kappa=0$) have been made in [42] using a different numerical method. Comparison with the present results showed good agreement and

presented a maximum discrepancy of 0.9% for various Reynolds numbers computed. The obtained numerical results are also similar to those obtained from Bashtovoy et al. for non conducting magnetic fluid (FHD). For the fully developed flow in a straight rectangular duct, under the action of an applied magnetic field, they observed that two vortices arose at the transverse plane, whereas the axial velocity was reduced [19]. As far as it could be investigated, there are no results documented in the literature concerning the influence of magnetic field on the flow of a biofluid in a curved duct.

RESULTS AND DISCUSSION

Figure 2 shows the axial velocity profiles (b column) and corresponding contours (a column) for different values of Mn , $Pz=-8000$ and for $\kappa=0$ (straight duct). For $Mn=0$ the contours of H are shown whereas for values of $Mn=3\times 10^6$ and 5×10^6 the stream function at the transverse plane is pictured (c column). The magnetic field is applied at the point $(x_s, y_s)=(-0.02, 0.5)$ and H_o is taken at $(x_o, y_o)=(0, 0.5)$. It is seen that as Mn increases, secondary flow arises at the transverse plane. The axial velocity reduces near the area where the magnetic field is applied and the secondary flow strengthens as the magnetic field strengthens. The secondary flow appears in the form of two symmetric counter-rotating vortices that are generated on each side of the $y=y_s$ horizontal line.

In Figure 3 different axial profiles are pictured (b column) for curvature $\kappa=0.25$, for various values of Mn and $Pz=-8000$. The magnetic field is applied at the point $(x_s, y_s)=(-0.02, 0.5)$ and (x_o, y_o) is taken at $(0, 0.5)$. The contours of the axial velocity and stream function are also pictured (a and c column, respectively). For $Mn=0$ the well-known profiles of the hydrodynamic flow inside a curved square duct appear. For $Mn=3\times 10^6$ it is seen that near the area of application of the magnetic field the axial velocity is retarded and the two vortices of the secondary flow are joined together in a similar manner to the $\kappa=0$ case. However these effects of the magnetic field are confined to the area close to the magnetic source, while the rest of the flow field retains

the characteristics of the previous case for $Mn=0$. For $Mn=5 \times 10^6$ the magnetic field is strengthened significantly and affects the whole flow field. The contours and the profile of the axial velocity (columns a and b, respectively) show that the axial flow is retarded in a wide area near the magnetic source and that the maximum values of the axial velocity are located close to the $y=y_s$ horizontal line, but do not lie on it. Concerning the transversal flow field (column c), the centres of the counter rotating vortices are shifted towards the source of the magnetic field, close to which the secondary velocities appear significantly increased.

Figures 4 and 5 show axial velocity profiles (column b) and contours plots (columns a and c) for the axial and transverse plane respectively for $Pz=-8000$. For these cases, namely $\kappa=0.1$ and 0.25 , the magnetic field is applied at the point $(x_s, y_s)=(1.02, 0.5)$ which is represented by the black dot in column c of Fig.4 and $H_o(x_o, y_o)$ is taken at $(1.00, 0.5)$. A first observation from Figs.4, 5 is that the area where the axial velocity is retarded, is transposed to the left side of the cross-section, following the relocation of the magnetic source, while the position of the maximum axial velocity is shifted towards the centre of the duct. Concerning the secondary flow, the behaviour described in Figs.4, 5 is altogether different from the one in the previous figures. In this case the magnetic source and the centre of the curvature are located on opposite sides of the duct. This results to the development of opposed and conflicting forces that act on the cross-sectional flow, which for $Mn=3 \times 10^6$ lead to the creation of two pairs of counter rotating vortices. The present pattern of the secondary flow also appears in the hydrodynamic flow in a curved square duct with absence of a magnetic field. In the “non-magnetic” case, bifurcations in the solution cause the secondary flow to form either two or four-vortex patterns depending on the curvature and the Reynolds number and this behavior has been attributed to the balance between the centrifugal and the axial pressure gradient forces. In the present problem, where there is presence of a magnetic field, the understanding of the phenomenon is more complicated since all three kinds of forces, centrifugal, axial pressure gradient and magnetic, contribute to the formation of the secondary flow patterns. Evidence of this, are the flow patterns for $Mn=5 \times 10^6$ in Fig. 4 for $\kappa=0.1$ and Fig.5 for $\kappa=0.25$, where three pairs of vortices arise in the secondary flow. It could be said that

the vortex pair that is near the magnetic source is mainly due to the magnetic field, while the aforementioned balance between the centrifugal and the axial pressure gradient forces creates the other two pairs. However, in order to solidify such an assertion, a detailed numerical calculation of the physical bifurcations would be required, a task that is out of the scope of the present work.

Figure 6 shows various axial velocity profiles (column b) and corresponding contours (columns a and c) for the axial and transverse plane respectively for $Pz=-8000$, $\kappa=0.1$. In this case the magnetic field is applied at the point $(x_s, y_s)=(0.5, -0.02)$ and $H_o(x_o, y_o)$ is taken at $(0.5, 0.0)$. It is observed that the symmetry of the flow ceases to exist and that, as on all of the previous cases, the axial velocity is retarded near the area of application of the magnetic field. It is also observed that the location of the maximum axial velocity is traced to the lower left quarter of the duct, very close to the area where the minimum axial velocity appears due to the magnetic field. The axial velocity profile between these locations of marginal velocities shows a very steep increase. Concerning the secondary flow it is seen that three vortices appear in all the cases of Fig.6. However, the one due to the magnetic field is limited in both extent and magnitude, and its effect on the cross-sectional flow is notable only in the case for $Mn=5 \times 10^6$.

Figure 7 shows the variation of Reynolds number with the axial pressure gradient $-Pz$ for curvatures $\kappa=0$ (straight duct), 0.1 and 0.25 and for magnetic numbers $Mn=0$ and 5×10^6 with the magnetic source located at $(x_s, y_s)=(-0.02, 0.5)$ and $H_o(x_o, y_o)$ taken at $(0, 0.5)$. It is observed that the variation of the Reynolds number with $-Pz$ is almost linear and that as the curvature increases the Re decreases. The effect of the magnetic field on Re is greater for small values of curvature, while for $\kappa=0.25$ the flow rate (Re) is not affected by the presence of the magnetic field. An interesting observation from the $\kappa=0.1$ curves is that application of the magnetic field causes the aforementioned bifurcation phenomenon of the secondary flow to appear for a lower axial pressure gradient than in the case of the “non-magnetic” flow (with $Mn=0$). It is seen that the “jump” that designates transition from two to three vortex pairs, appears in the $\kappa=0.1$ and $Mn=0$ curve for $Pz=-5 \times 10^4$ while in the $\kappa=0.1$ and $Mn=5 \times 10^6$ curve for $Pz=-3 \times 10^4$. This fact shows the effect of the magnetic field on the overall force balance and the resulting flow patterns.

In order to investigate the influence of the magnetic field in the flow, for different values of the magnetic number Mn , the number $Re^*=100((Re-Re_o)/Re_o)$ is defined, where Re_o is the Re number for $Mn=0$.

Consequently, Re^* represents the percentage change of Re due to the presence of the magnetic field.

The variation of Re^* with the curvature κ , for different positions of application of the magnetic field and for $Mn=0, 3\times 10^6$ and 5×10^6 is shown in Figure 8. It is observed that in general Re^* decreases as the curvature increases. Moreover, the greatest percentage decrement of Re^* with the curvature occurs for the hydrodynamic flow ($Mn=0$). This decrement reaches almost 27.5% for $\kappa=0.25$. For $Mn=3\times 10^6$ the differences in Re^* for the various locations of the magnetic source are comparatively small and a minimum Re^* of -17% is reached for $\kappa=0.25$. For stronger magnetic field with $Mn=5\times 10^6$, Re^* is affected less, but the choice of the position of the magnetic field plays more significant role. Especially in the cases of application of the magnetic field at the points $(x_s,y_s)=(1.02, 0.5)$ and $(0.5, -0.02)$ the flow is accelerated for relatively small curvatures ($\kappa<0.1$). This acceleration is greater for $(x_s,y_s)= (0.5, -0.02)$ and reaches almost 5% for $\kappa\approx 0.04$. For $\kappa>0.1$ the flow is retarded and irrespective of the position of the magnetic source Re^* reaches approximately -7% for $\kappa=0.25$. As a general observation it can be concluded that the application of the magnetic field opposes to the tendency of the reduction of the flow rate with the curvature. Moreover, the flow can be accelerated for a relatively high Mn and a relatively small curvature ($\kappa<0.1$) and the location of the magnetic source affects mainly the produced flow patterns of the velocities and not the flow rate itself, with few exceptions.

Figure 9 shows the variation Re^* with the magnetic number Mn for different positions of the magnetic source, for curvatures $\kappa=0, 0.1$ and 0.25 and for axial pressure gradient $Pz=-8000$. For convenience in the following context the location of the magnetic source will be indicated by the abbreviation LS when it is positioned at the left side of the duct at $(x_s,y_s)=(-0.02, 0.5)$, by RS when it is at the right side at $(x_s,y_s)=(1.02, 0.5)$ and by BS when it is at the lower side at $(x_s,y_s)= (0.5, -0.02)$. From the examination of Fig.9 it is observed that the greater variation of Re^* with the increment of the magnetic number Mn occurs for the straight duct ($\kappa=0$) and for $Mn=5\times 10^6$ it reaches -24%. For $\kappa=0.1$ and the LS case the decrement of Re^* is

significantly less and reaches 7% for $Mn=5 \times 10^6$. For all other computed the reduction of Re^* does not exceed -4.5%. Concerning the variation of Re^* it is seen that for the LS and BS cases, Re^* presents an essentially linear dependence with Mn for $Mn > 10^6$. For the RS case the behavior of Re^* is different and presents a slight increase for low Mn , followed by a decrease for medium values of Mn . However the variation is small and remains within $\pm 2\%$.

CONCLUSIONS

For the straight duct ($\kappa=0$) as the magnetic number Mn increases, secondary flow in the form of two vortices arises at the transverse plane. The axial velocity reduces near the area where the magnetic field is applied and the secondary flow strengthens as the magnetic field strengthens. For the case of the curved duct the position of the magnetic source plays important role for the formation of the flow field. Depending on the position of the source the vortices at the transverse plane can alter in form, change in number or become asymmetric. The axial velocity changes significantly with the application of the magnetic field and is retarded close to the area of the magnetic source. For a specific curvature, increase of the magnetic field results to a decrease of the flow rate. This effect of the magnetic field is dependent on the value of the curvature and Re^* reduces as the curvature increases.

The present results were obtained using the simplified mathematical model of BFD based on the principles of FHD. There are several issues that could be investigated in future studies. Adopting a new model that would take into account the non-Newtonian properties of blood, its ionic nature (electrical conductivity), and the “apparent” viscosity due to the application of the magnetic field could aid a better understanding of biomagnetic fluid flow. However, these first results using the adopted simplified mathematical model reveal considerable influence of the magnetic field on blood flow and encourage further studying for possible medical and engineering applications.

ACKNOWLEDGEMENTS

The authors wish to thank the referees for their comments which helped to improve their article.

References

- [1] Y. Haik, V. Pai and C. J. Chen, “Development of magnetic device for cell separation”, *Journal of Magnetism and Magnetic Materials* **194**, 254-261 (1999).
- [2] J. M. R. Carlton, C. A. Yowell, K. A. Sturrock and J. B. Dame, “Biomagnetic separation of contaminating host leukocytes from plasmodium-infected erythrocytes”, *Experimental Parasitology* **97**, 111-114 (2001).
- [3] P. A. Voltairas, D. I. Fotiadis, L. K. Michalis, “Hydrodynamics of magnetic drug targeting”, *Journal of Biomechanics* **35**, 813-821 (2002).
- [4] Ch. Alexiou, A. Schmidt, R. Klein, P. Hulin, Ch. Bergemann and W. Arnold, “Magnetic drug targeting: biodistribution and dependency on magnetic field strength”, *Journal of Magnetism and Magnetic Materials* **252**, 363–366 (2002).
- [5] Y. Haik, C. J. Chen and J. Chatterjee, “Numerical simulation of biomagnetic fluid in a channel with thrombus”, *Journal of Visualization*, **5**, 2, 187-195 (2002).
- [6] J. Plavins and M. Lauva, “Study of Colloidal Magnetite Binding Erythrocytes: Prospects for Cell Separation”, *Journal of Magnetism and Magnetic Materials*, **122**, 349-353 (1993).
- [7] T. Higashi, A. Yamagishi, T. Takeuchi, N. Kawaguchi, S. Sagawa, S. Onishi and M. Date, “Orientation of Erythrocytes in a strong static magnetic field”, *J. Blood* **82**, 4, 1328-1334 (1993).
- [8] C. Gasparovic and N. A. Matweiyoff, “The Magnetic Properties and Water Dynamics of the Red Blood Cell”, *Magnetic Resonance in Medicine*, **26**, 274-279 (1992).
- [9] A. N. Shaylgin, S. B. Norina and E. I. Kondorsky, “Behaviour of Erythrocytes in High Gradient Magnetic Field”, *Journal of Magnetism and Magnetic Materials* **31**, 555-556 (1983).
- [10] T. Takeuchi, T. Mizuno, A. Yamagishi, T. Higashi and M. Date, “Orientation of red blood cells in high magnetic field”, *Journal of Magnetism and Magnetic Materials* **140-144**, 2, 1462-1463 (1995).

- [11] T. Higashi, N. Ashida, and T. Takeuchi, "Orientation of blood cells in static magnetic field", *Physica B*, 616-620 (1997).
- [12] L. Pauling and C. D. Coryell, "The magnetic Properties and Structure of Hemoglobin, Oxyhemoglobin and Carbonmonoxy Hemoglobin", In *Proceedings of the National Academy of Science, USA*, **22**, 210-216 (1936).
- [13] Y. Haik, V. Pai and C. J. Chen, "Biomagnetic Fluid Dynamics, In: *Fluid Dynamics at Interfaces*", W. Shyy and R. Narayanan (Eds.), Cambridge University Press, 439-452 (1999).
- [14] M. Motta, Y. Haik, A. Gandhari and C. J. Chen, "High magnetic field effects on human deoxygenated hemoglobin light absorption", *Bioelectrochemistry and Bioenergetics* **47**, 2, 297-300 (1998).
- [15] M. Bartoszek, and Z. Drzazga, "A study of magnetic anisotropy of blood cells", *Journal of Magnetism and Magnetic Materials* **196-197**, 573-575 (1999).
- [16] S. Ichioka, M. Minegishi, M. Iwasaka, M. Shibata, T. Nakatsuka, K. Harii, A. Kamiya and S. Ueno, "High-intensity static magnetic fields modulate skin microcirculation and temperature in vivo", *Bioelectromagnetics* **21**, 3, 183-188 (2000).
- [17] Y. Haik, V. Pai and C. J. Chen, "Apparent viscosity of human blood in a high static magnetic field", *Journal of Magnetism and Magnetic Materials* **225**, 180-186 (2001).
- [18] Y. Haik, J. C. Chen and V. M. Pai, "Development of bio-magnetic fluid dynamics", In *Proceedings of the IX International Symposium on Transport Properties in Thermal Fluids Engineering*, Singapore, Pacific Center of Thermal Fluid Engineering, S.H. Winoto, Y.T. Chew, N.E. Wijesundera, (Eds.), Hawaii, U.S.A., June 25-28, 121-126 (1996).
- [19] V. G. Bashtovoy, B. M. Berkovsky and A. N. Vislovich, "Introduction to thermomechanics of magnetic fluids", Hemisphere publishing co., Springer-Verlang (1988).
- [20] B. Berkovski and V. Bashtovoy, "Magnetic fluids and applications handbook", Begell house inc., New York (1996).

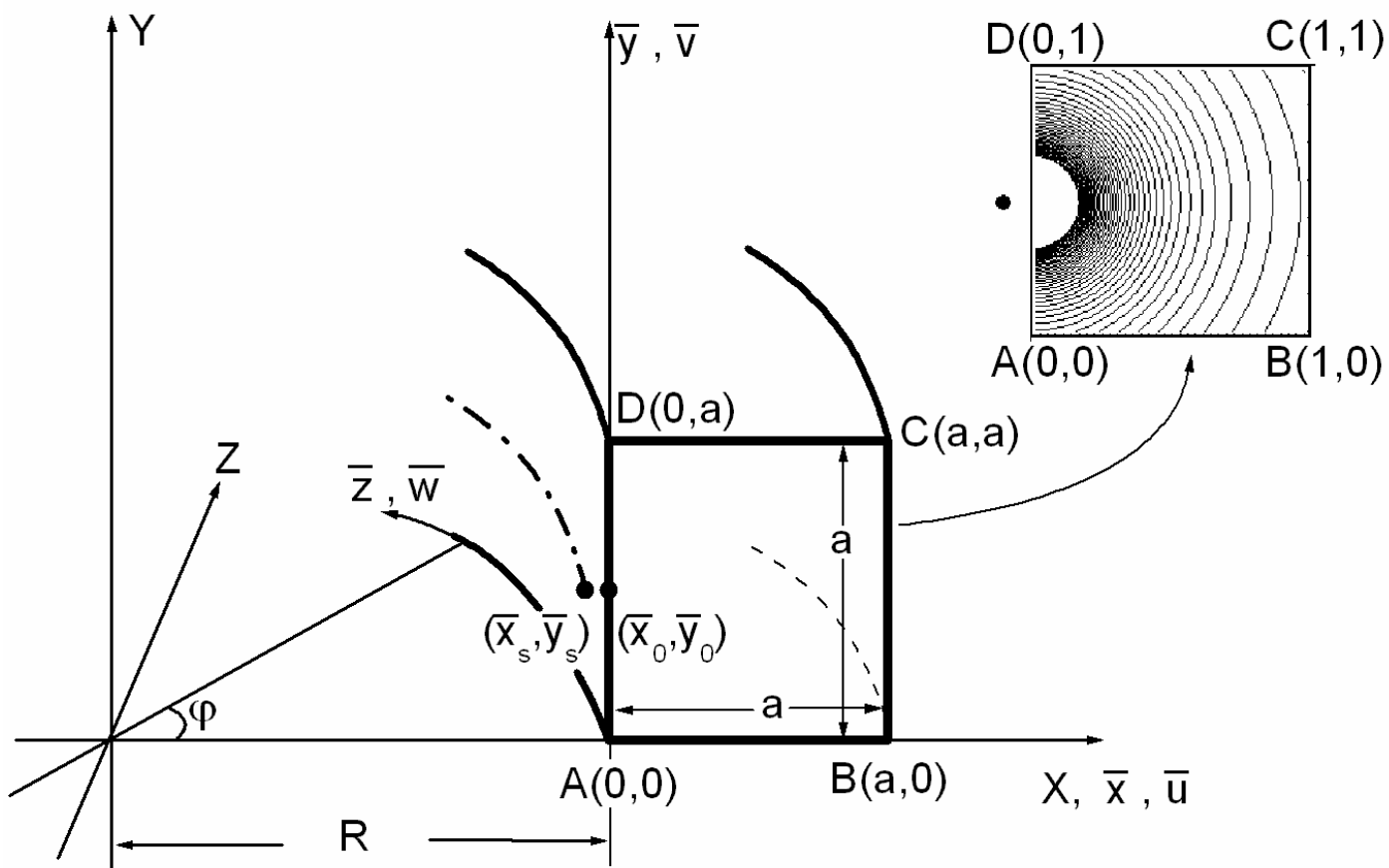
- [21] E. Blums, A. Cebers and M. M. Maiorov, "Magnetic Fluids", Walter de Gruyter, Berlin (1997).
- [22] V. E. Fertman, Magnetic fluids guidebook: properties and applications, Hemisphere publishing co., New York (1990).
- [23] J. L. Neuringer and R. E. Rosensweig, "Ferrohydrodynamics", Physics of Fluids, **7**, 1927-1937 (1964).
- [24] R. E. Rosensweig, "Ferrohydrodynamics", Cambridge University Press (1985).
- [25] R. E. Rosensweig, "Magnetic fluids", Ann. Rev. Fluid Mech. **19**, 437-463 (1987).
- [26] R.A. Frewer, "The electrical conductivity of flowing blood", Biomedical Engineering, 552-554 (1974).
- [27] F. Jaspard and M. Nadi, "Dielectric properties of blood: an investigation of temperature dependence", Physiological Measurement, **23**, 547-554 (2002).
- [28] S. Gabriel, R.W. Lau and C. Gabriel, "The dielectric properties of biological tissues: III. Parametric models for the dielectric spectrum of tissues", Physics in Medicine and Biology, **41**, 2271-2293 (1996).
- [29] K.R. Cramer and S.I. Pai, "Magnetofluid dynamics for engineers and applied physicists", Scripta Publishing Company, Washington D.C. (1973).
- [30] W.F. Hughes and F.J. Young, "The Electromagnetodynamics of Fluids", John Wiley & Sons, Inc. New York, 1st Ed. (1966).
- [31] G.W. Sutton and A. Sherman, "Engineering Magnetohydrodynamics", McGraw-Hill, Inc. New York (1965).
- [32] K. C. Cheng, R. C. Lin and J.W. Ou, "Fully developed laminar flow in curved rectangular channels", ASME, J. Fluids Eng., 41-48 (1976).
- [33] G. J. Hwang and C. H. Chao, "Forced laminar convection in a curved isothermal duct", ASME J. Heat Transfer, **113**, 48-56 (1991).
- [34] K. N. Ghia, U. Ghia and C. T. Shih, "Study of fully developed incompressible flow in curved ducts using a multigrid technique", ASME J. Fluids Eng., **109**, 226-235 (1987).

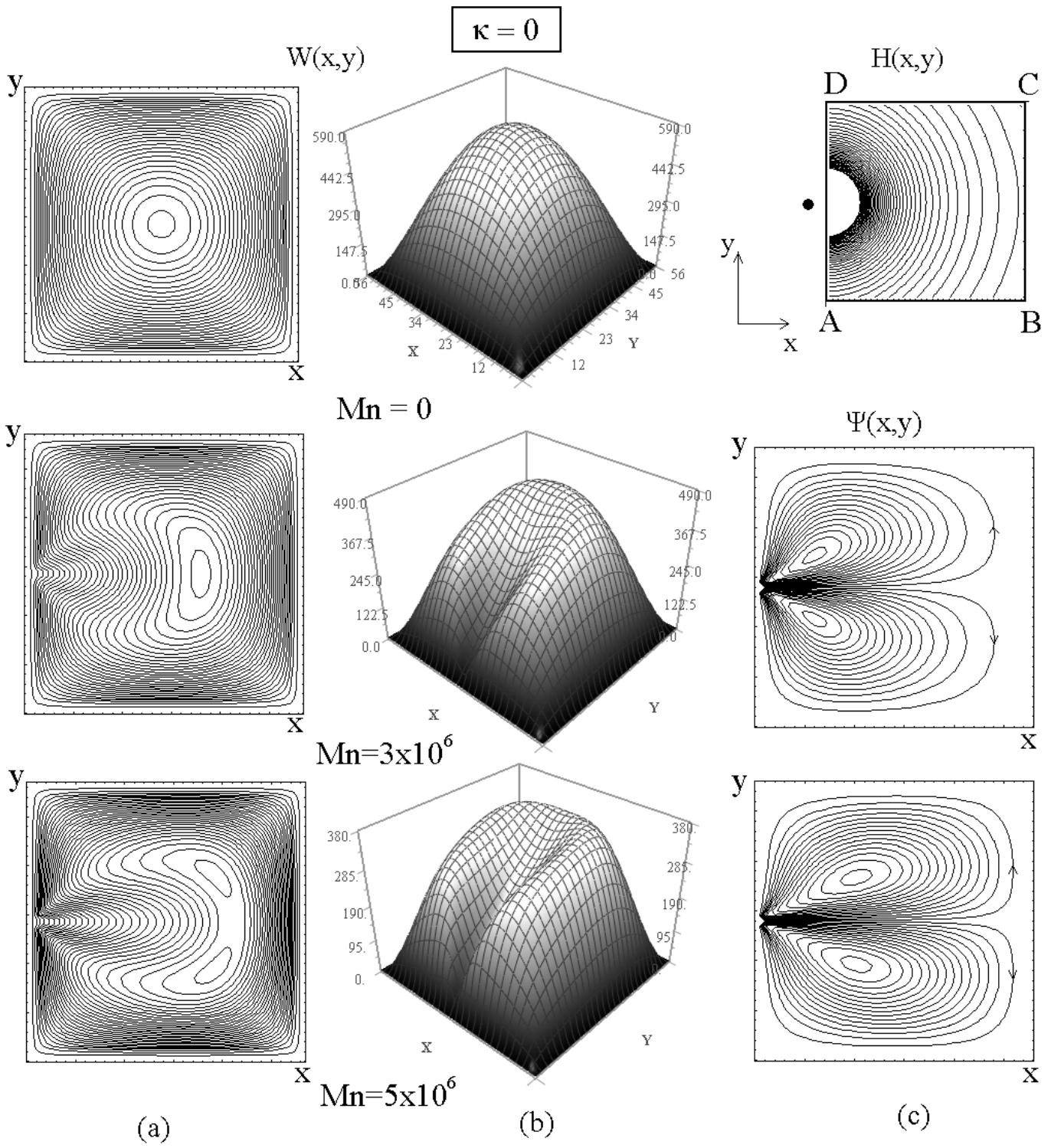
- [35] S. Thangum and N. Hur, "Laminar secondary flows in curved rectangular ducts", *JFM*, **217**, 421-440 (1990).
- [36] V. D. Sakalis V.D. and P. M. Hatzikonstantinou, "Predictions and accuracy of the CVP numerical method for the developed laminar flow in curved ducts", in Proceedings of the 4th GRACM Congress on Computational Mechanics, University of Patras, 1400-1406 (2002).
- [37] K. H. Winters, "A bifurcation study of laminar flow in a curved tube of rectangular cross-section", *J. Fluid Mech.*, **180**, 343-369 (1987).
- [38] W. Shantini and K. Nandakumar, "Bifurcation phenomena of generalized Newtonian fluids in curved rectangular ducts", *J. Non-Newtonian Fluid Mech.*, **22**, 35-59 (1986).
- [39] W. Y. Soh, "Developing fluid flow in a curved duct of square cross-section and its fully developed dual solutions", *J. Fluid Mech.*, **188**, 337-361 (1988).
- [40] P. Hille, R. Vehrenkamp and E. O. Schulz-Dubois, "The development and structure of primary and secondary flow in a curved square duct", *J. Fluid Mech.*, **151**, 219-241 (1985).
- [41] B. Bara, K. Nandakumar and J. H. Masliyah, "An experimental and numerical study of the Dean problem: flow development towards two-dimensional multiple solutions", *J. Fluid Mech.*, **224**, 339-376 (1992).
- [42] E.E. Tzirtzilakis, V.D. Sakalis, N.G. Kafoussias and P.M. Hatzikonstantinou, "Biomagnetic fluid flow in a 3D rectangular duct", *International Journal for Numerical Methods in Fluids*, (accepted).
- [43] G.R. Zendehebudi and M.S. Moayeri, "Comparison of physiological and simple pulsatile flows through stenosed arteries", *Journal of Biomechanics*, **32**, 959-965 (1999).
- [44] H.I. Andersson, R. Halden and T. Glomsaker, "Effects of surface irregularities on flow resistance in differently shaped arterial stenoses", *Journal of Biomechanics*, **33**, 10, 1257-1262 (2000).
- [45] S. V. Patankar, "Numerical Heat Transfer and Fluid Flow", McGraw-Hill, New York (1980).

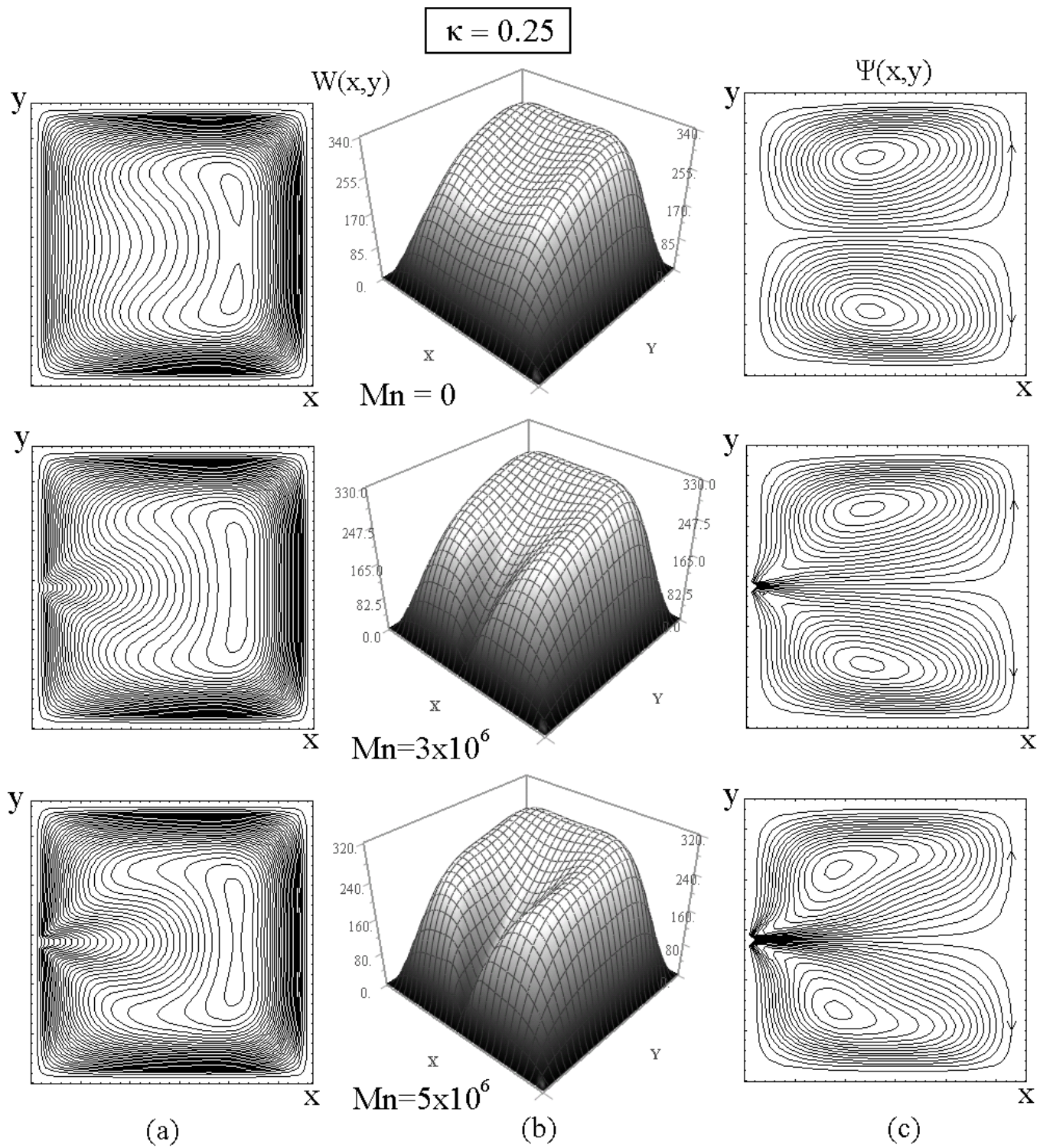
- [46] P. K. Papadopoulos and P. M. Hatzikonstantinou, “Effects of various numerical methods on the formation of the secondary flow in a curved square duct”, in Proceedings of the 4th GRACM Congress on Computational Mechanics, edited by D.T. Tsahalis, University of Patras, 750-758 (2002).
- [47] T. J. Pedley, “The fluid mechanics of large blood vessels”, Cambridge University Press (1980).

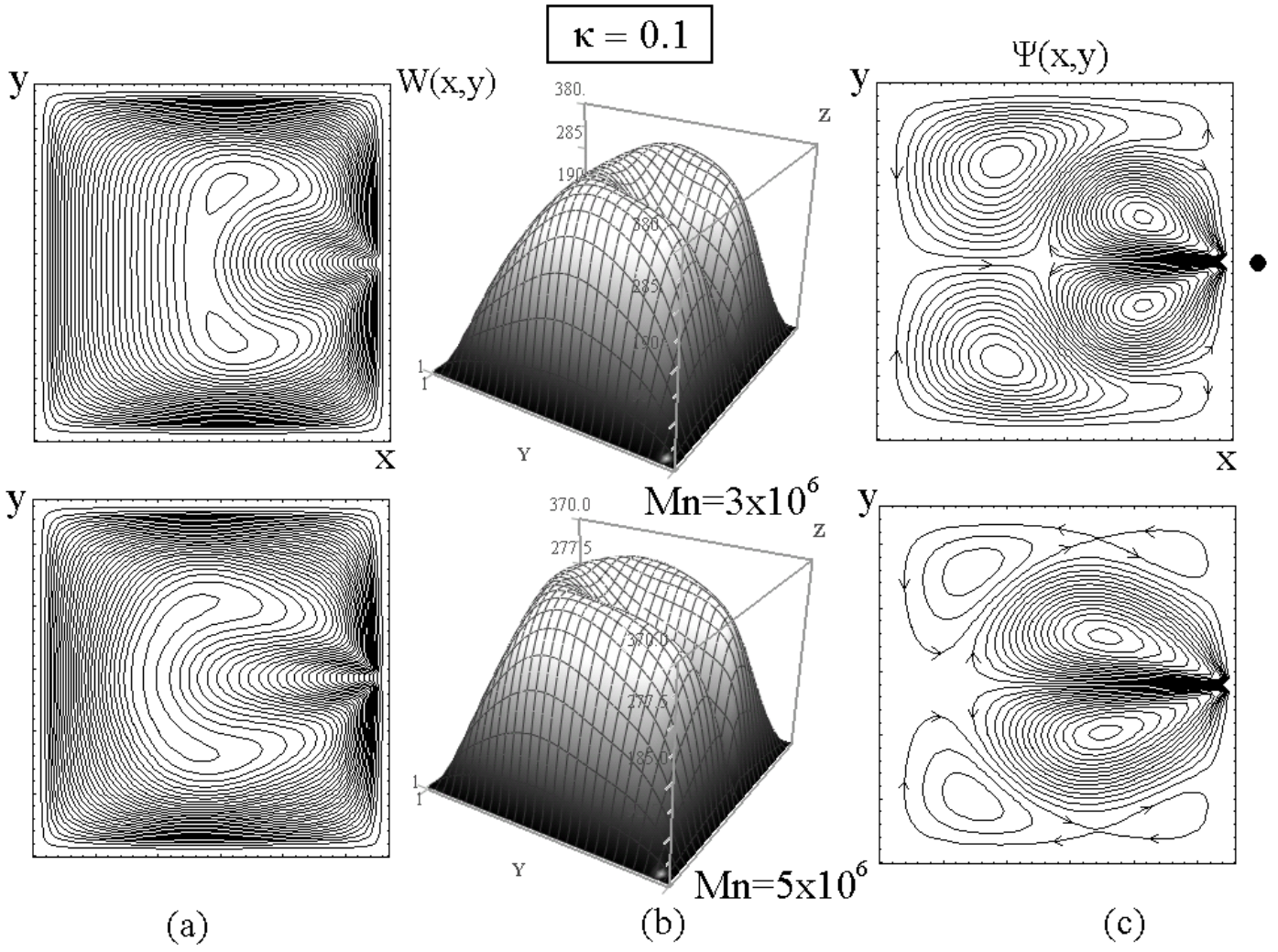
Captions of Figures

- Figure 1:** The flow configuration. The contours of the spatially varying magnetic field of strength H are shown in the ABCD plane of the cross section where the flow is studied.
- Figure 2:** Axial velocity profiles (b column) and corresponding contours (a column) for different values of Mn and for $\kappa=0$ (straight duct). For $Mn=0$ the contours of H are shown whereas for the other values of Mn the stream function at the transverse plane is pictured (c column).
- Figure 3:** Axial velocity profiles (b column) and corresponding contours (a column) for different values of Mn and for $\kappa=0.25$. The stream function contours at the transverse plane are shown in c column.
- Figure 4:** Axial velocity profiles (b column) and corresponding contours (a column) for different values of Mn and for $\kappa=0.1$. The stream function contours at the transverse plane are shown in c column. The magnetic field is placed at the point $(x_s, y_s)=(1.02, 0.5)$
- Figure 5:** Axial velocity profiles (b column) and corresponding contours (a column) for different values of Mn and for $\kappa=0.25$. The stream function contours at the transverse plane are shown in c column. The magnetic field is placed at the point $(x_s, y_s)=(1.02, 0.5)$
- Figure 6:** Axial velocity profiles (b column) and corresponding contours (a column) for different values of Mn and for $\kappa=0.1$. The stream function contours at the transverse plane are shown in c column. The magnetic field is placed at the point $(x_s, y_s)=(0.5, -0.02)$
- Figure 7:** Variation of Re with axial pressure gradient $-Pz$ for various values of κ and Mn .
- Figure 8:** Variation of Re^* with curvature for various values of Mn and for different positions (x_s, y_s) of the magnetic source.
- Figure 9:** Variation of Re^* with Mn for various curvatures and different positions (x_s, y_s) of the magnetic source.

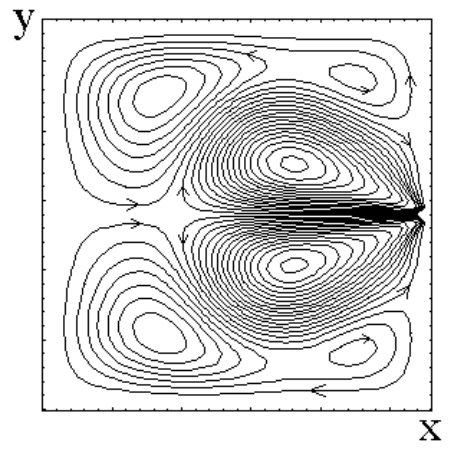
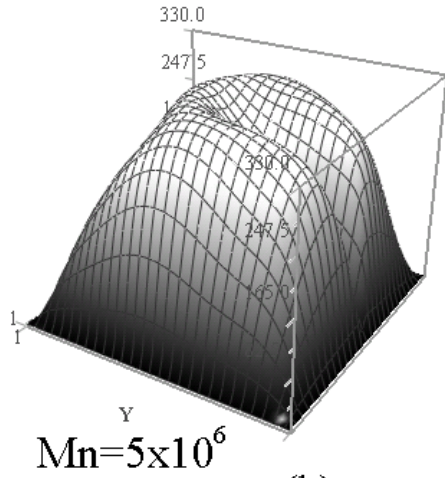
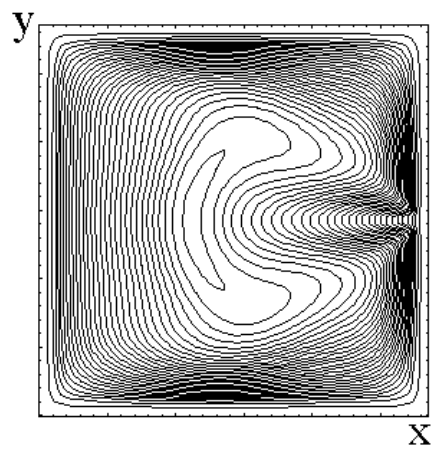
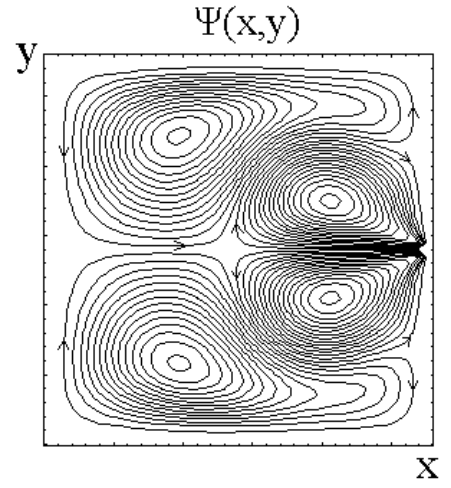
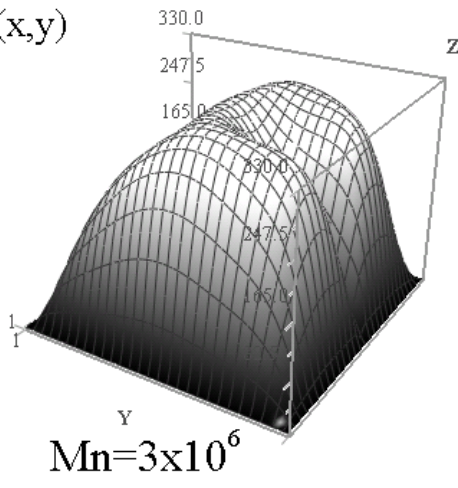
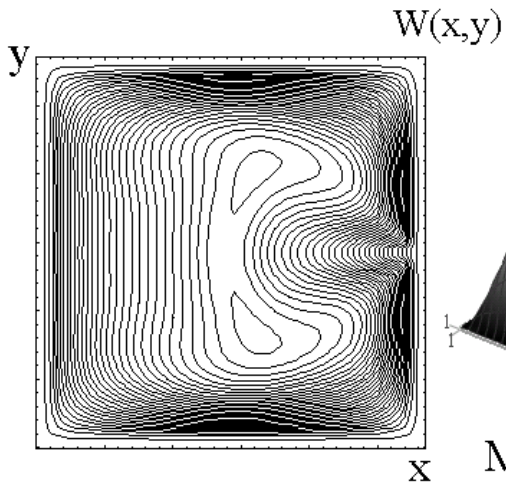








$\kappa = 0.25$



(a)

(b)

(c)

$\kappa = 0.1$

